Approach for modelling thermoplastic generative designed parts

Florian Althammer[1,2], David Moncayo[1] and Prof. Dr.-Ing. Peter Middendorf[2]

[1]Daimler AG, Research and Development, Sindelfingen, Germany
[2]IFB Institute of Aircraft Design, University of Stuttgart, Germany

1 Abstract

This study presents an approach to characterize thermoplastic generative designed parts and compares the usability of different material models in LS-DYNA.

For using 3D printed parts in prototypes it is at first necessary to be able to predict the deformation behaviour of the printed part itself. The deformation behaviour of thermoplastics and especially of thermoplastic generated parts depends on a variety of material properties. In general the parts have a composed anisotropy consisting of the process and material anisotropy. The process anisotropy is reflected to different mechanical properties due to the building directions of the 3D printer. The material anisotropy includes divergent tension and compression behaviour and approximately orthotropic behaviour due to particle reinforcement. The main task therefore is to evaluate current material routines and modeling techniques to ensure the predictability of the parts behaviour with available and implemented material cards.

The performed characterization consists standard specimen tests for a non-reinforced and a carbon particle reinforced thermoplastic, which is produced in the selective laser sinter process. The conducted tests are a tensile, a compression and a shear test. The test specimen were built in different construction directions. In addition, component tests were executed in order to evaluate the predictability of the generated material cards in multiaxial stress states.

KEYWORDS: **material characterization, thermoplastic, selective laser sintering**

2 Introduction

Over the last years, a great effort can be seen in developing and improving additive manufacturing processes. The aim is to ensure the quality and the reproducibility of the printed parts on a high level. Despite the great dependence of several process and material parameters, printed prototype parts have a certain quality level, which includes only small scattering of material properties [1]. This capability of additive manufacturing makes it attractive for the automotive industries. Not only to build up fast and geometrically independent prototypes but also to use them in functional assemblies to evaluate structures in experimental tests.
The need of dimensioning the prototypes and the experimental tests leads to a strong interest in describing the material behaviour of the used 3D printed parts. The conducted experiments include a broad spectrum of different loading and bearing conditions. Most of the experiments consider the parts' stiffness in quasistatic loading conditions. These tests can be extended in order to investigate the large displacement and failure behavior of the parts. Other tests vary the velocity of the loading to examine the strain rate behaviour of the regarded specimen. The aim of modeling these tests with finite elements is therefore to get the most precise approximation of the appeared physical effects. Due to limited computing capacity of the finite element analysis, in a first assumption the used element types and the needed solver are chosen depending on the nonlinearity of the regarded experiments. In addition, the selection of the material model and the referenced material cards is influenced by the defined discretization of the FE-model and the available material data. The effort to calibrate material cards is expensive especially when several material cards are needed to calculate different test scenarios.

In Table 1 a brief overview of non-reinforced and reinforced thermoplastics, their process and the resulting mechanical behaviours are listed.

Material	Polymer Type	Production Process	Filler	Elastic Modulus [MPa]	Tensile Strength [MPa]	Break Elongation [%]
Duraform GF (3DSystem)	PA12	SLS	Glass beads	4068	26	1,5
PA2200 (EOS)	PA12	SLS	-	1650	48	18
	PA12	Injection Molding	-	1500	280	
Ultrasint X028 (BASF)	PA6	SLS	-	3550	78	13
	PA6	Injection Molding	-	3000	80	70
ABS-M30 (Stratasys)	ABS	FDM	-	2230	28	2
	ABS	Injection Molding	-	2300	45	10

Table 1: Overview of mechanical properties of thermoplastics in manufacturing processes [2,3,4,5]

Depending on the 3D printing method used, the 3D printing material properties almost reach or exceed the characteristic values compared to the reference process, the widely used injection molding.

The aim of this paper is therefore, according to the recently published studies of Reithofer [6] for thermoplastics], to also illustrate the available methods and the usability of different material cards for 3D printed parts and various experiments.

3 Comparison of recent available material cards

With the consideration of fiber reinforced plastics in vehicle crash simulations, more and more material cards appear, which represent the anisotropy in material behaviour. At first, the focus of material modeling layed on the anisotropy of the stiffness matrix. The material cards have been extended over the time in order to include more regions of the total mechanical properties [7]. The second step was to take a closer look on the behaviour of thermoplastics, with the development of **`*MAT_187`** (**`*MAT_SAMP`**). In the last years, the material cards **`*MAT_157`** has been improved to illustrate the behaviour of short-fiber reinforced thermoplastics [8]. Nevertheless, all the developed and validated material cars had a focus on crash test scenarios, whereas the finite element model includes shell formulations and the used solver was based on a explicit time integration method.

Due to the diverse process and material dependent material properties of thermoplastic 3D printed parts, the aim of the calculation is to approximate as many of the physical effects as possible. Furthermore, there is still the risk to build up material cards for only one special test case, which is afterwards not usable in other finite element models or calculation disciplines. Therefore, the following Table 2 represents an overview of common material cards with a focus on the possibility to also use them in implicit calculations or in combination with solid element types.

Material Card	Anisotropic Elastic Modulus	Anisotropic pl. Strain	Yield surface	Strain rates	Damage model	Element Formulation	Implicit/ Explicit
`*MAT_024`	No	No	v. Mises	Yes	Fail strain GISSMO	Shell /Solid	Imp./Exp.
`*MAT_086`	Yes	No	*Not available*	No	GISSMO	Shell	Exp.
`*MAT_103_P`	No	Yes	Hill	No	GISSMO	Shell /Solid	Imp./Exp.
`*MAT_108`	Yes	Yes	orthotropic	No	GISSMO	Shell	Exp.
`*MAT_124`	No	No	v. Mises (Tension&Compression)	Yes	Fail strain GISSMO	Shell/Solid	Imp./Exp.
`*MAT_157`	Yes	Yes	Hill	Yes	GISSMO	Shell/Solid	Imp./Exp.
`*MAT_187`	No	No	Triaxiality dependent	No	GISSMO	Shell/Solid	Exp.
`*MAT_215`	Yes	(yes)	unknown	Yes	Fail strain DIEM	Shell/Solid	Exp.

Table 2: Comparison of the applicability of available material cards for plastics [9]

The table demonstrates the broad range of possible material cards for 3D printed materials. Each of them has its own specialization in describing defined regions of the complex thermoplastic behaviour. Unfortunately, the cards are not applicable for every element formulation or every available solver in LS-DYNA. An advantage of the cards in most cases is the possibility to add **`*MAT_ADD_EROSION`** in

order to extend the description of the failure as well as the damage behaviour with the available GISSMO or DIEM damage models.
To start with, in this paper the following material cards have been analysed in order to be able to predict the mechanical properties of 3D printed parts:

1) ***MAT_024**
2) ***MAT_124**
3) ***MAT_157**
4) ***MAT_187**

The cards are in general used with shell formulations and explicit analysis. As a reference, for a small amount of simulations, solid elements and implicit solver are also considered.

4 Experimental Setup

The experimental characterization has been conducted for a non-reinforced polyamide 12 (NRT) and a particle reinforced polyamide 12 (RT) material, which are both used in selective laser sinter processes. Although the materials absorb less than one percent of humidity, both have been conditioned in order to ensure an equivalent balance of humidity. In Figure 1 the used test specimen are illustrated.

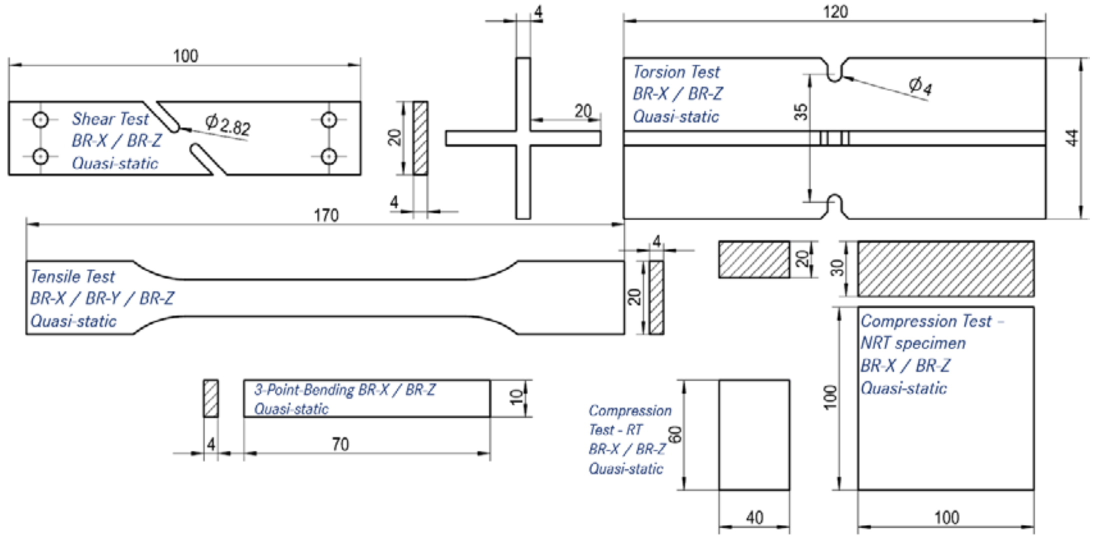

Fig.1: Overview of used test specimen in the characterization

On the coupon level tension, compression, shear and three-point bending test specimen are tested. In order to represent multi axial stress states a newly developed notched cross rip structure is tested in a torsion experiment.
The building direction and the positioning of the test specimen in the printing chamber can influence the resultant mechanical properties of the parts. Therefore, the characterization considers different arrangements of the test specimen and evaluates the need of consideration in the material cards. In Figure 2, the two assembly spaces of the 3D printers with the placed specimen are shown.

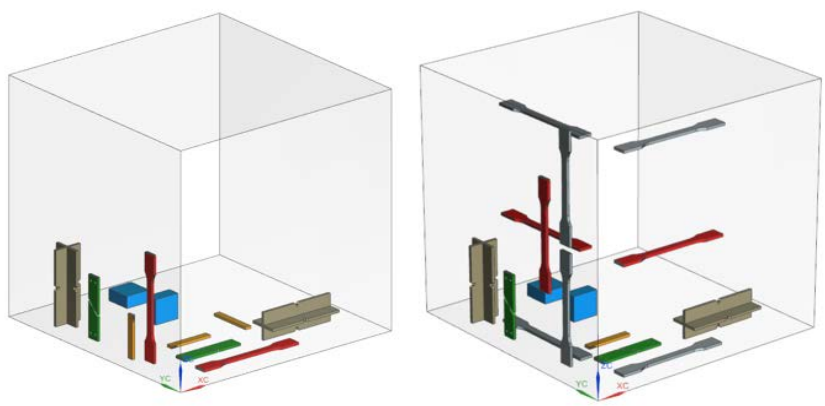

Fig.2: Assembly space of the non-reinforced (NRT,left) and the reinforced SLS material (RT,right)

The assembly space of the two 3D printers has been subdivided in three vertical spaces, which are designated ,,TOP'', ,,MID'' and ,,DOWN''. The specimen are labelled by their geometry principal axis and how the axis is positioned in the printing process. If a specimen is for example printed in ,,X-direction'', then the specimen lies on the X-Y-plane of the printer with its thickness in ,,Z-direction'' . In further illustrations they are abbreviated by ,,BR-X''.
With this test assembly of specimen a first estimation of the resultant mechanical behaviour can be achieved. In this first evaluation strain rate dependencies have not been considered. The configuration of the experimental characterization is listed in Table 3.

Material	Test specimen	Building directions (BR)	Positions	Thickness	Velocity
Non-reinforced PA12 (NRT)	Tensile/Compression/ Shear/3-P-Bending/ Notched cross rip	X / Z	Down	4 mm	Quasi-static [0.001 1/s]
Reinforced PA12 (RT)	Tensile	X / Y / Z	Top / Mid / Down	4 mm	Quasi-static [0.001 1/s]
	Compression/ Shear/ 3-Point-Bending/ Notched cross rip	X / Z	Down	4mm (3PB: 2mm)	Quasi-static [0.001 1/s]

Table 3: Overview of the test specimen composition

This configuration is a compromise between a general configuration for non-reinforced thermoplastics and the comprehensive test for anisotropic (short-fiber) reinforced thermoplastics. It is also a compromise between the printing costs of the first assembly and the possibility to submit further smaller and less expensive printing jobs to evaluate selected regions of the mechanical behaviour.

5 Experimental Results

The experiments are conducted with different measuring systems. In general, the tests contain a load cell and an extension sensor in order to extract the force-displacement-curves. The results of the tests are described in the following section.

Tensile test
In the tensile test, the NRT specimen show a rather isotropic behaviour in the elastic region and a significant anisotropic behaviour in the plastic strain region. Although the BR-X specimen show a high deformation behaviour, the fracture surface is more brittle than ductile. The test configuration is shown in Figure 3.

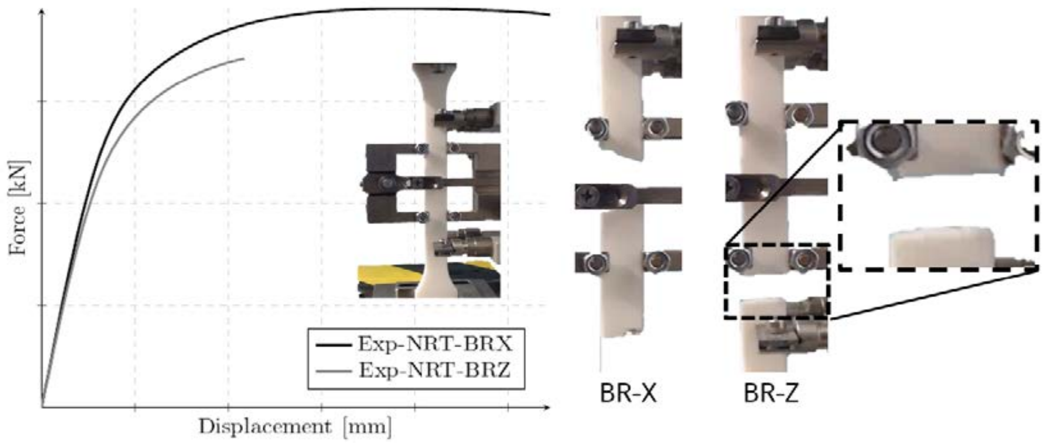

Fig.3: Experimental results and test setup of tensile tests with NRT

In contrast, the RT specimen show an inverted mechanical behaviour with a pronounced orthotropic elastic and less marked anisotropic plastic strain region. Different strain states can be located just before the fracture of the specimens. The optical measurement of the strains in main specimen axis reveal for every building direction different strain regions. The common fracture behaviour of non-reinforced thermoplastics, which is represented through a homogenous strain state right until the final fracture occurs, is shown at the BR-Y specimen. The BR-X and BR-Z specimens have tension stripes, which lead to a rather locally defined fracture. Especially the BR-Z specimen have significant areas of the divergent strains.

This behaviour can be clearly attributable to the sintering process and its layered structure. The resulting force-displacement-curves and the measured strains are shown in Figure 4.

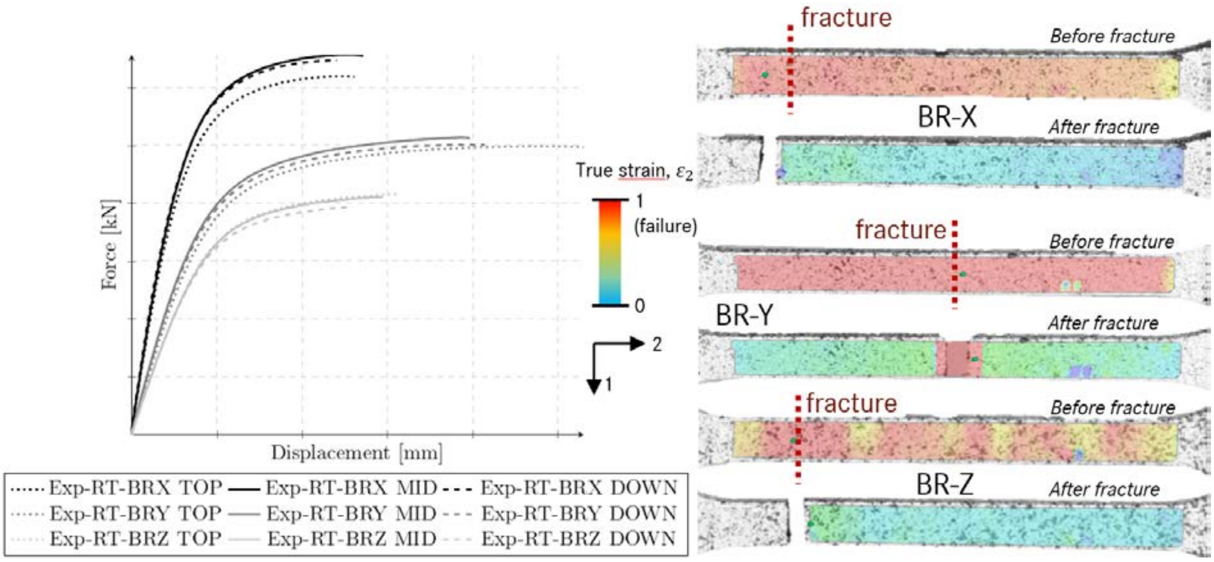

Fig.4: Experimental results and strain states measured with digital image correlation of the RT

Compression test

The compression tests contain two types of cuboidal blocks with different dimensions. The aim was to ensure a broad homogenous stress cross-section. Consequently, the results constitute an average behaviour of the local inhomogeneities. However, the dimensioning of the compression specimen did not seem to be the best solution. After reaching the maximum compression stress, a slipping of the specimen occurs so that no constant stress state could be reached. For calibration purpose of the material cards only the deformation until maximum pressure can be used. The results of the compression test are shown in Figure 5.

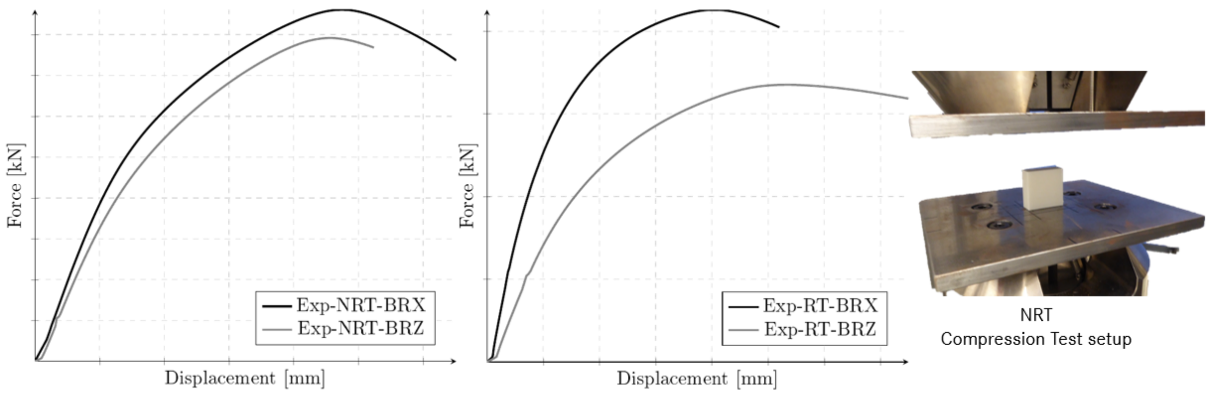

Fig.5: Experimental results and test setup of the compression test for NRT (left) and RT (right)

Nevertheless a rather isotropic for the NRT and a pronounced anisotropic for the RT compression behaviour could be determined. Due to the layered structure of the BR-Z specimen, a less stiff compression modulus and a lower maximum compression force is reached. Especially with the BR-Z specimen of the RT the maximum strength is shifted to higher compression strains.

Shear test

Over the years several shear test specimen were developed and calibrated to evaluate the simple and pure shear behaviour of thermoplastic. The tests were conducted either on standard tensile test machines or on special shear test systems. According to the GISSMO material models for metals [10], which include a defined set of test specimen, a shear test specimen with 45° rotated shear-cross section area were used. The specimen can be tested with standard tensile test machines, so that no additional tools or test instruments are needed. To extract the force-displacement-curves the machines load cell and a macroscopic extension sensor are used. The relevant data for the material cards, like the shear modulus and the shear stress, can be extracted and calculated afterwords. The results of the shear tests are illustrated in Figure 6. To start with, the building directions BR-X and BR-Z are examined. This setup allows an initial evaluation of the suitability of the test specimen and secondly the determination of the materials shear behaviour. In contrast to the tensile test results, both materials show a distinct dependency of the building direction and the resulting force-displacement curves.

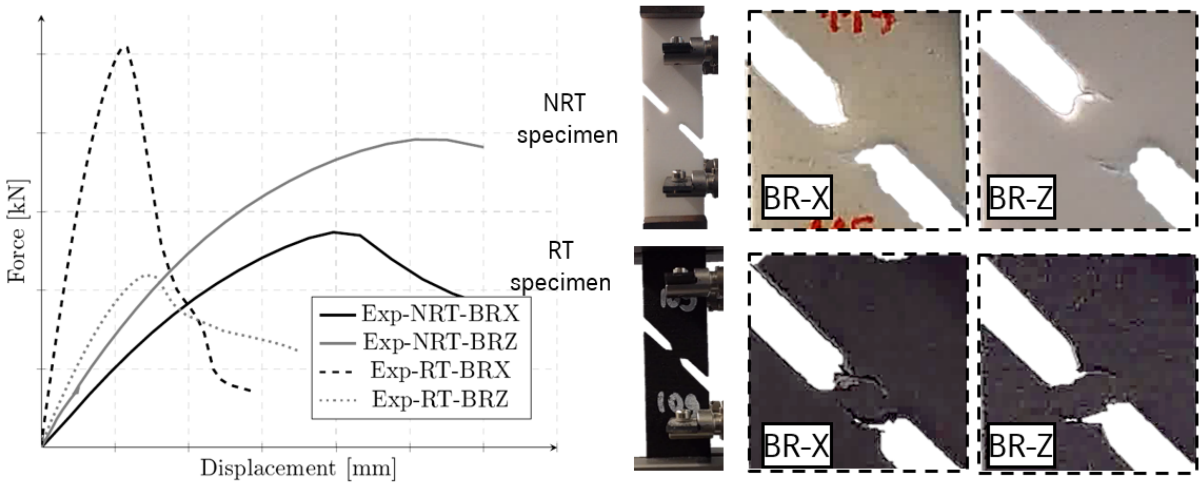

Fig.6: Experimental results and test setup for the shear test specimen (NRT, white; RT, black)

3-Point Bending test

Three-point bending tests help to illustrate the dependencies of the tension and compression states in materials. In addition, the tests are generally used to calibrate simple and complex material cards in order to achieve a quite well assumption of the thermoplastic tension and compression anisotropy. Although the test is only suitable for strains with a maximum of 5 % [11], both investigated materials have been tested. Due to the high fracture strain of the NRT, the determined test results aren't suitable to calibrate the fracture behaviour of the NRT material models. The test results are shown in Figure 7.

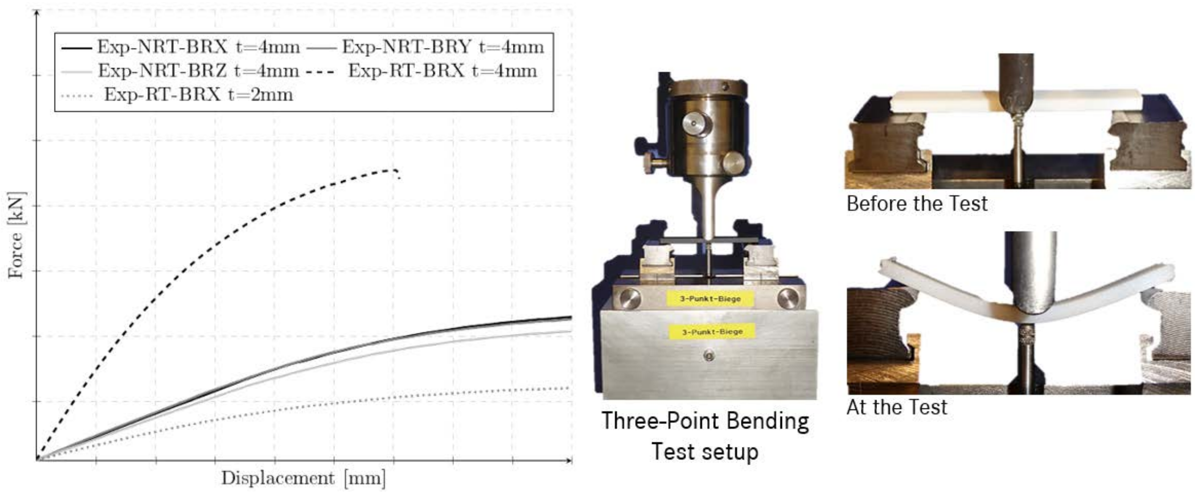

Fig.7: Experimental results and test setup of the 3-Point Bending test

Besides the two building directions of the NRT specimen, also the third direction has been considered in this test. The results show that no relevant deviations between the BR-X and the BR-Y specimen could be measured. With higher deformation, the behaviour of the BR-X and BR-Y specimen deviate from the BR-Z specimen. The focus of the three-point bending test with the RT specimen did not lay on the building direction but on the specimen thickness. While in the other tests the specimen had a thickness of four millimetres, here the RT specimen are printed both in BR-X direction with a thickness of two and four millimetres. These results are suitable to get a first estimation of the thickness dependency of the built up material models.

Torsion test
The last conducted experiment is used to examine the materials behaviour in multi-axial stress states, which occur for example in ripped structures. A special test device has been developed to mount the cross-rip specimen. The bearing is made with four triangle shaped blocks, which are pressed against the specimen. While one side of the tools is kept fixed, the other side rotates with a predefined velocity of one degree per second. The test device contains a load cell, which is mounted on a robot arm. The robotic interface allows to extract the torque-rotations-curves of the experiment. The resulting curves and the test device are illustrated in Figure 8.

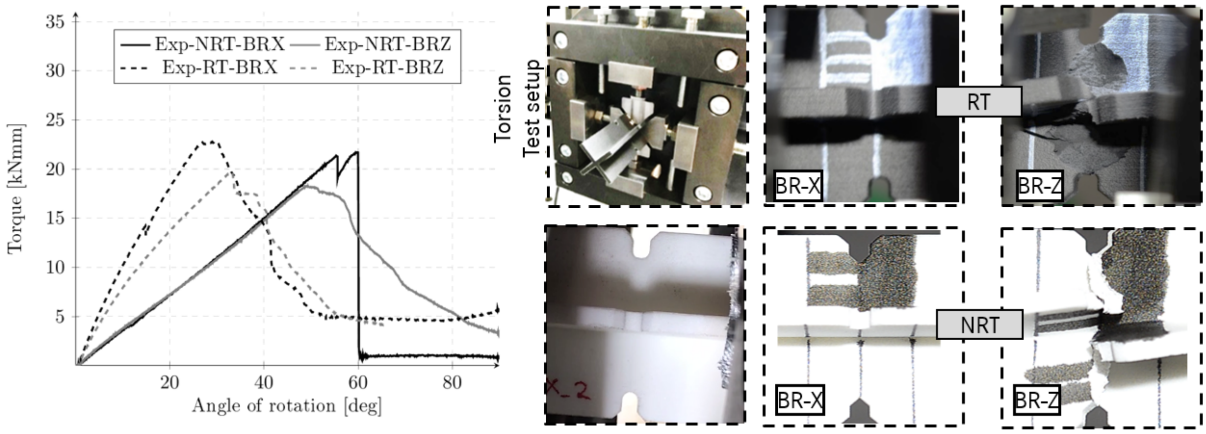

Fig.8: Experimental results and test setup for the notched cross-rip specimen

The results demonstrate once more the isotropic and anisotropic behaviour of both materials. For small rotation angles both materials have an building direction-independent torsion stiffness. With increasing rotation angles, the anisotropy of the RT in the elastic region and the anisotropy of the NRT in the plastic region can be determined.

6 Simulation Setup

The regarded experiments consist of specimen with a general thickness of four millimetres. This thickness dimension constitutes a transition area, which still allows the use of shell formulation or already allows, considering calculation time, the discretization with solid elements. The choice of an appropriate finite element for this simulation task includes in general shells, thick shells or solid elements. Fortunately, the chosen material cards from Table 1, allow the switch of the element formulation later on. To start with, the shell formulation with fully integrated elements (element form 16) is selected. The element size for all specimen is defined as two millimetres. The generated meshes for the specimen are shown in Figure 9.

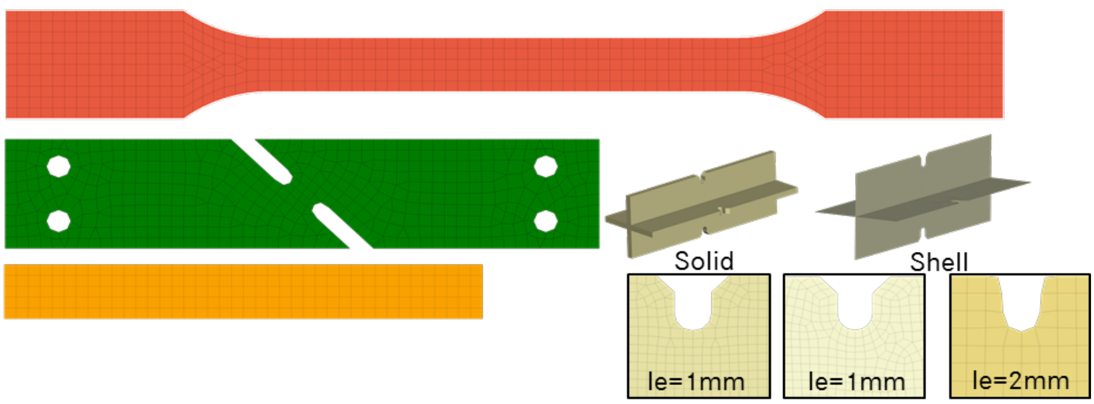

Fig.9: Overview of specimen mesh with shell and solid elements

In order to illustrate the influence of the chosen element type for the regarded simulation, the cross-rip specimen is also modelled with solid elements with two different mesh sizes. Although a mesh size of two millimetres leads to a high aspect ratio in the used shell compression specimen, the mesh size was not adjusted. After setting up the finite element models, the input data for the chosen material is defined. In Table 4 the chosen configuration of the material cards is shown.

Nr.	Material	LS-DYNA Mat. No.	Element Type	Load Curves	Solver	Damage/ Failure model
1	NRT	*MAT_024	Shell	LCSS Tension BRX	exp.	GISSMO
2	NRT	*MAT_124	Shell	LCSS Tension/Compression BRX	exp.	GISSMO
3	NRT	*MAT_187	Shell	LCSS Tens./Compr./Shear BRX	exp.	
3b	NRT	*MAT_187	Shell	LCSS Tens./Compr./Shear BRX	exp.	GISSMO
4	RT	*MAT_24	Shell	LCSS Tension BRX	exp.	GISSMO
5	RT	*MAT_124	Shell	LCSS Tension/Compression BRX	exp.	GISSMO
6	RT	*MAT_157	Shell	LCSS Tension BRX	exp.	GISSMO
7	RT	*MAT_157	Solid	LCSS Tension BRX	exp.	GISSMO
8	RT	*MAT_157	Solid	LCSS Tension BRX	imp	GISSMO

Table 4: Configuration of the built-up material cards

There are different methods available for the calibration of material cards in order to approximate predefined stress state scenarios. The calibration of the model depends on how many input data a material card needs and how the missing physical behaviour, which cannot be displayed with a certain material card, is approximated. With the variety of conducted tests and the several dependent material behaviours, the aim was to set a default base configuration for all models. So the material cards could be evaluated afterwords. Therefore, the NRT and the RT material cards are build-up with true stress-strain load curves of the building direction with the higher mechanical data. As solver, the explicit MPP is used with the version 9.3. To use the same solver for implicit analysis the solver was set to double precision in advance.

GISSMO model

In contrast to high ductile materials, where the GISSMO model can achieve a high level of approximation in damage modeling, the regarded materials show a minor ductile necking behaviour. Therefore, only a low-level GISSMO modeling setup was chosen. At first, GISSMO was defined as a two dimensional material card, although it is also used in the solid models afterwords. The used damage parameters were:

```
IDAM = 1       FADEXP = 1
DMGTYP = 1     LCSDG = Defined curve
DMGEXP =1      ECRIT = Defined curve
```

With this configuration the simple strain based failure model of a **`*MAT_024`** can be replaced with a triaxiality dependent failure model so that a higher approximation of the fracture behaviour can be achieved.

`*MAT_157` and the Hill Criterion

In addition to the summary from Reithofer [6] of common material models for plastics, the already in Table 2 mentioned **`*MAT_157`**, can predict the deformation behaviour of plastics. Its particular feature was first used for metal sheet simulations where anisotropy is induced through the rolling direction of the sheets. With the developed yield criterion of Hill in 1948, it was possible to define anisotropic yield surfaces based on the ratios of the yield stresses of the three regarded directions [12]. In equation 1 the yield criterion is described as

$$F(\sigma_{22}-\sigma_{33})^2 + G(\sigma_{33}-\sigma_{11})^2 + H(\sigma_{11}-\sigma_{22})^2 + 2L\sigma_{23}^2 + 2M\sigma_{31}^2 + 2N\sigma_{12}^2 = 1 \qquad (1)$$

The constants F, G, H , L, M and N represent further equations, which include the ,,R'' constants. The constant F is for example defined as

$$F = ½ (1/R_{22} + 1/R_{33} - 1/R_{11}) \qquad (2)$$

while R_{11} is the ratio between the σ_{11}-yield stress and the reference yield stress. The R-constants are in general labelled to the three anisotropy principal directions. In modelling thermoplastics the R-constants are used to describe the resultant deformation behaviour depending on the local fiber-orientation degree [12]. For the used shell elements the constants R_{00} and R_{90} are relevant to define the anisotropic yielding behaviour. Regarding the 3D printed parts, the anisotropy is defined globally parallel to the building directions.

7 Simulation Results

Tensile Test

The NRT tensile test simulation with the ***MAT_024** and ***MAT_124** cards shows a high level of approximation. In combination with the ***MAT_ADD_EROSION** the deformation and failure behaviour reached a good convergence to the experimental results. The ***MAT_187**, which at first has no defined failure, shows an increasing force over the displacement. The evaluation of the RT tensile test simulations shows an equal behaviour of all three regarded material cards. Due to the implemented stress-strain-curve of the BR-X experimental result, the plastic strain and fracture behaviour could be approximated with only a small deviation. In addition, the two other directions could be calculated with iterated orthotropic stiffness parameters and the Hill-parameters R00 and R90 of ***MAT_157,** which define the yield ratios for the two shell element directions [13]. The used isotropic GISSMO damage model was not able to calculate the anisotropic fracture strains of the RT. This effect poses, especially for the BR-Z specimen, a clear disadvantage. A high deviation between the simulated and the measured failure strain was the result. In Figure 10 the behaviour of the regarded material cards in the tensile test are illustrated.

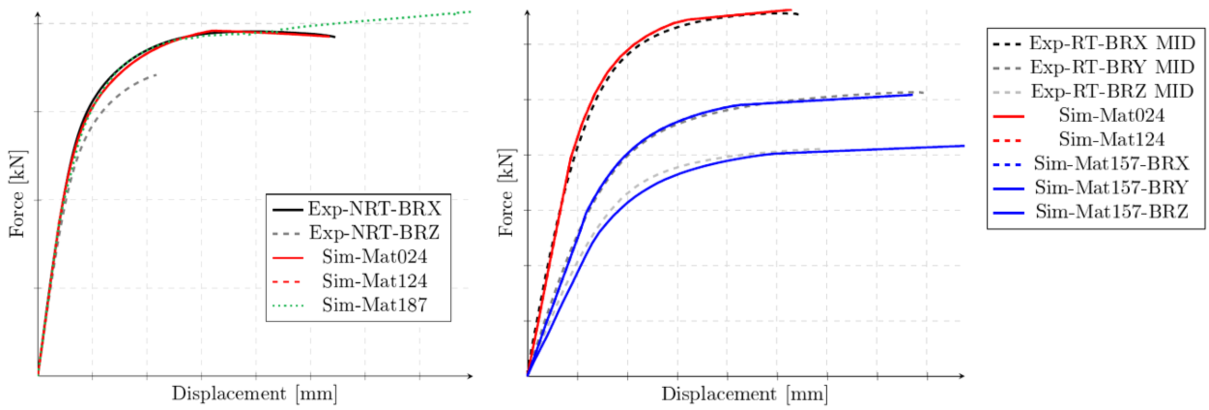

Fig.10: Simulation results of tensile tests for NRT and RT test specimen

Although this paper regards only FE-models with mesh sizes of two millimetres, further tensile test were conducted to evaluate the mesh sensitivity of the built-up ***MAT_024** material cards. In Figure 11 the determined regularization curves, the resulting localization behaviour of the meshes and their fracture points are illustrated.

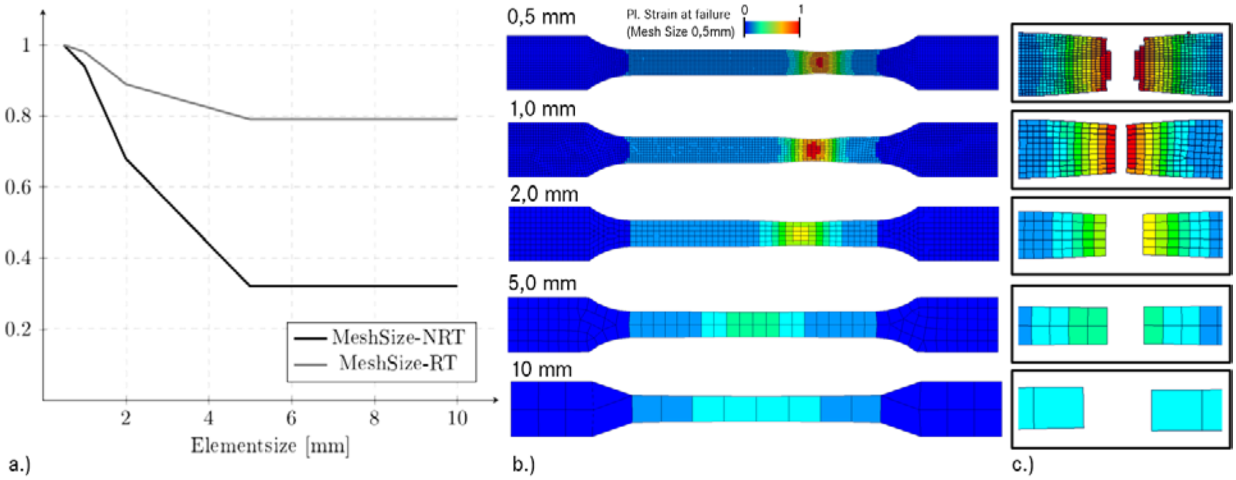

Fig.11: Defined curves for mesh size regularization in GISSMO (a), pl. strain behaviour of NRT specimen in tensile test before (b) and after fracture (c)

The used GISSMO model can implement defined curves, which describe the relation between the damage and failure behaviour and the used element size. With the in built field ,,**LCREGD**'', the size dependent regularization factors for equivalent plastic strain to failure are defined.

Due to the particularly high elongation of the NRT specimen, a high scale factor in the regularization of the failure behaviour is needed. In contrast to the NRT specimen, the RT material card needed only a low level of regulation. The different models also reveal the localisation behaviour with rising element sizes. From the detailed necking in the zero point five millimetre mesh model to the broad homogenous elongation in ten millimetre model the different localization types and the absolute failure strains are shown.

Compression

The simulation of the compression test points out the limits of each material card in the possibility of prediction the materials behaviour. The main task, to depict the reduced compression stiffness and the higher strength in the plastic region, could only be considered with **`*MAT_124`**. The next closest convergence with the experimental results could be obtained with the **`*MAT_187`**. The standard material card **`*MAT_024`** describes the compression behaviour with a higher elastic stiffness and lower compression strength. The anisotropic tension and compression modulus can also be seen in the RT compression simulation, where especially the BR-Z specimen was calculated significantly to stiff. The results of the compression simulations are shown in Figure 12.

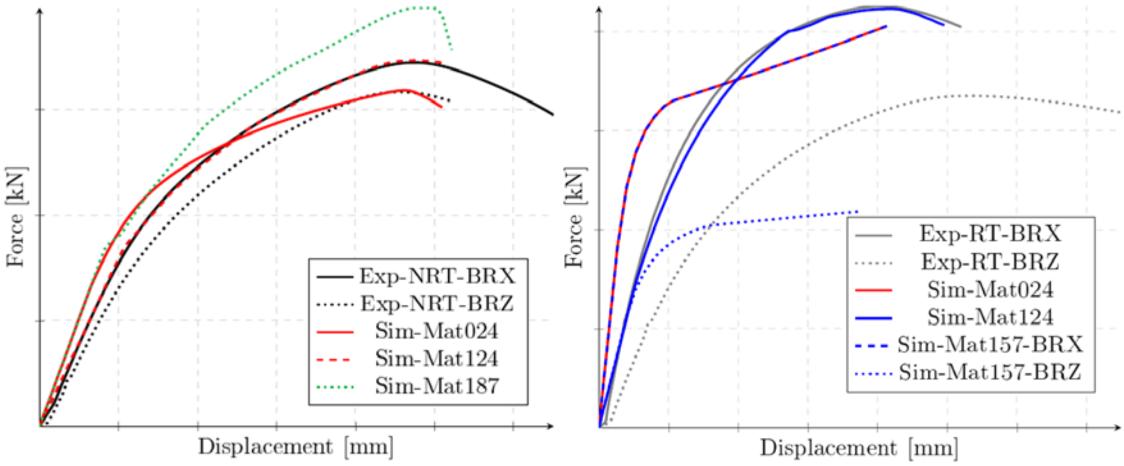

Fig.12: Simulation results of compression tests for NRT and RT test specimen

Shear Test

While simulating shear behaviour only the **`*MAT_187`** is able to implement stress-strain-based data in order to control a triaxiality dependent behaviour. An overview of the simulation results is given in Figure 13.

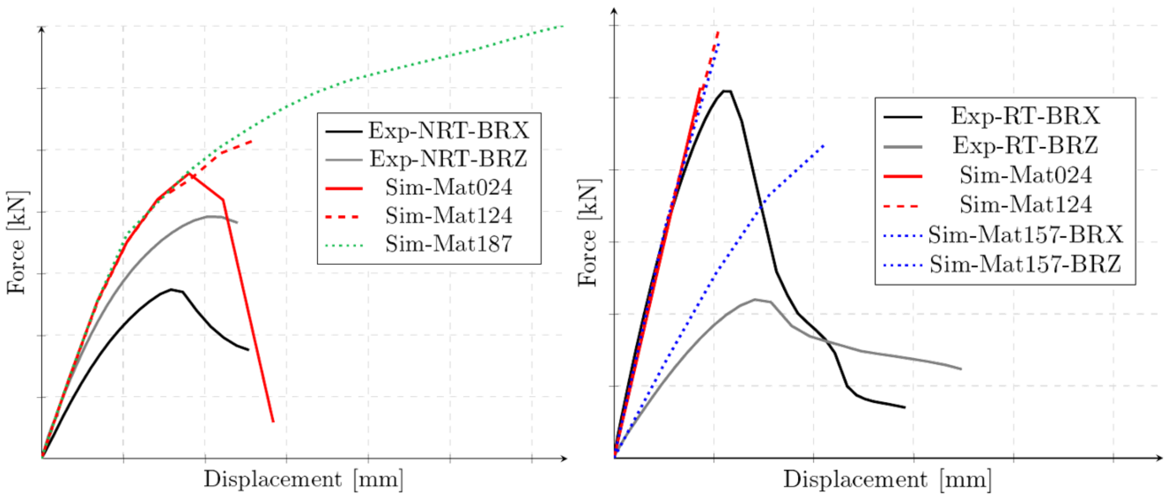

Fig.13: Simulation results of shear tests for NRT and RT test specimen

The shear behaviour of the NRT and RT shows a small region of elastic strain following with plastic and damage behaviour. Due to the used simplified GISSMO model, no extended damage behaviour could be modelled. The necking point could only be approximated at the maximum taken shear strength. Furthermore, the isotropic material cards ***MAT_024** and ***MAT_124** described the shear behaviour too stiff and calculated a 25 % higher maximum shear force. The anisotropic ***MAT_157** could also only approximate the specimen stiffness in BR-X and BR-Z direction, but failed in describing the plastic behaviour.

3-Point-BendingTest

With three-point bending tests, the built-up material cards are evaluated in terms of the predictive power they can achieve. The test induces a stress state, which superposes tension and compression loads. Material cards like ***MAT_024** can therefore be modified to average the tension and compression behaviour. Considering the regarded material cards the achieved results, based on the coupon tests earlier, are illustrated in Figure 14.

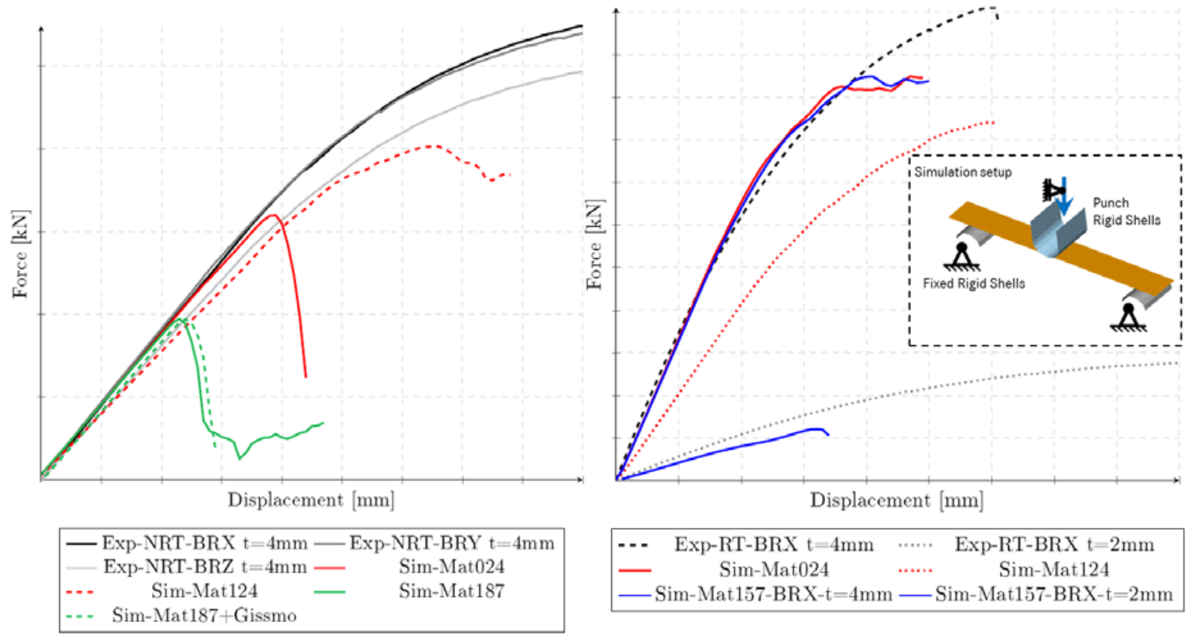

Fig.14: Simulation results of three-point bending tests for NRT and RT test specimen

The simulation results for the NRT clearly reveal the boundaries of every material card. The difference between the ***MAT_024** and the ***MAT_124** in describing compression stress states is demonstrated in the resulting maximum bending force. The built up ***MAT_187,** which showed an average approximation in the previous experiments, now reaches only a third of the maximum bending force. Nevertheless all three cards can fit the bending stiffness for small displacements. Due to the smaller anisotropy ratio between tension and compression, the bending behaviour of the RT can be described more precisely. Although the ***MAT_124** fits the previous compression results, a significant deviation of the bending behaviour occurs in the three point bending test. The tension data based cards ***MAT_024** and ***MAT_157** though both reach a higher level of prediction.

Notched cross-rip Test

The torsion test of the notched cross rips offers the opportunity to compare the different regarded material cards in a complex stress state scenario. The material cards, which are calibrated on coupon level, are used in the torsion simulation without any further averaging or calibration. The given quality of calibration of each material card can be examined in the test. The aim of this simulation was not to reach a high level of convergence with the experimental results. The simulation should rather demonstrate the trend behaviour of the material cards with the chosen finite element modeling of the mounting and loading case. The FE model is based on a ***CONSTRAINED_NODAL_RIGID_BODY**, which assigns the torsion velocity on a node set. In order to extract the resulting axial moments, the rip end is mounted with an ***Automatic_Surface_to_Surface_Contact** to a rigid shell. To simulate the torsion test two finite element models are defined. In general, there is for a comparison issue the shell discretization with an element size of two millimetres. Furthermore there are, as already presented in Figure 9, models with solid element of element sizes with one and two millimetres length. In addition, the implicit solver has been used to calculate the deformation behaviour in combination with a solid model and the anisotropic ***MAT_157**.

Again ***MAT_024** and ***MAT_124** reach a close approximation of the experiment in the first third of the deformation. Regarding the maximum calculated forces, the ***MAT_124** calculated higher torque moment than the ***MAT_024**. The simulation with an element size of one millimetre and the ***MAT_024** only divers in a small region to the two millimetres model. However, all three NRT cards were not able to calculate the significant higher torque moment at fracture. As already occurred in the three point bending test the ***Mat_187** did not reach the total displacement force in the torsion at all. In order to show its ability the GISSMO model of ***Mat_187** (*labelled with Sim-Mat 187-Gissmo**) was modified with a three times higher failure strain in compression state. This small modification leads to the plotted torque-rotation-curve, which depict the experimental maximum torque. The simulation results for the torsion test of the notched cross rip with the NRT and the two different FE models are shown in Figure 15.

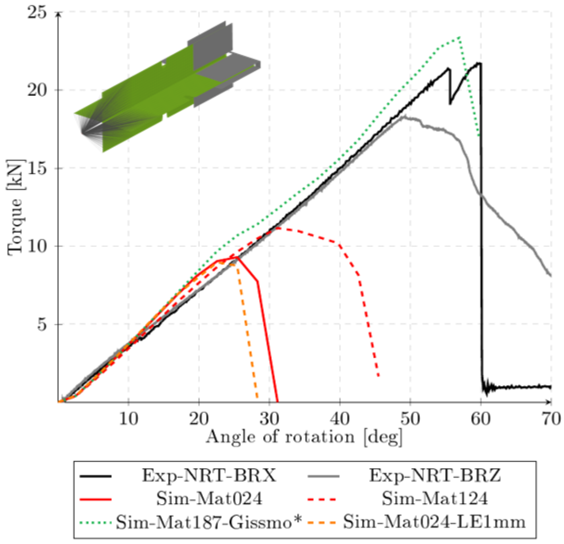

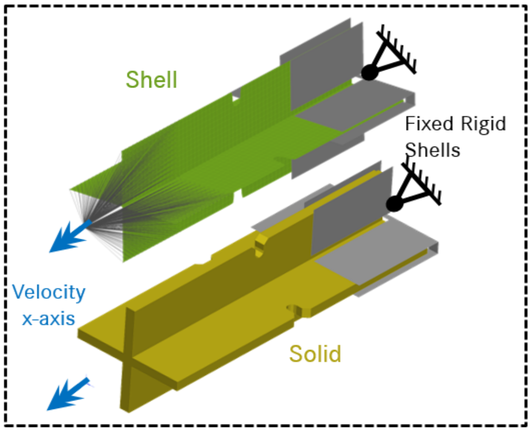

Finite Element Modell of notched cross rip torsion test

Fig.15: Simulation results of the torsion tests for NRT test specimen with shell model and overview of used FE-models of the notched cross rip specimen

The simulations of the RT specimen also show the limits of the regarded material cards. The calculated curves for the different FE models are shown in Figure 16.

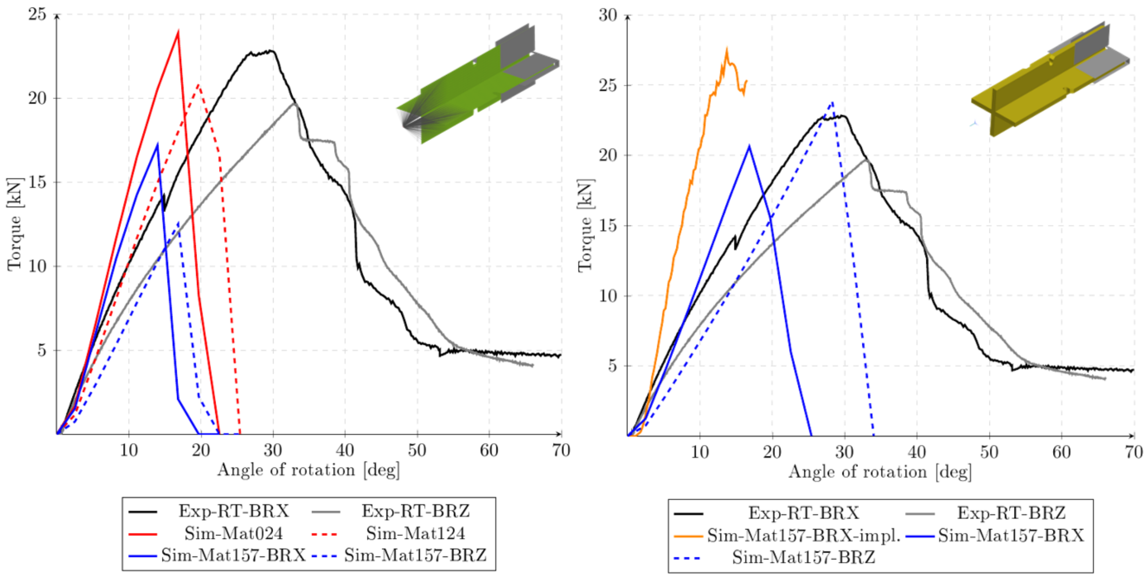

Fig.16: Simulation results of the torsion tests for RT test specimen with a shell model (left) and with solid models (right)

Each of the three used material cards show a good approximation on single parts of the total displacement. While the anisotropic ***MAT_157** depicts the elastic and plastic deformation behaviour for small rotation angles, the ***MAT_024** reaches a higher level of calculated torque and the ***MAT_124** has a better description of the plastic behaviour for the BR-X specimen shortly before fracture. This rather brittle behaviour can also come from the finite element modeling and the used contact definition. The significant stiff behaviour is also shown in the solid element variants. The finer mesh of the solid model leads to a higher computed torque, especially for the BR-Z specimen. The highest resulting torque and torsion stiffness is generated by the one millimetres solid model, which was computed with implicit solver.

8 Conclusion

The simulation of 3D printed parts requires a first determination of the range of anisotropy of the regarded materials. It has to be clarified, which of the predominant anisotropies are significant for the deformation behaviour. If the materials show a high influence in tension and compression anisotropy the building directions can be neglected and the isotropic material cards like ***MAT_124** and ***MAT_187** can approximate the material behaviour in a quite well average. If the material behaves rather brittle and shows a highly anisotropic behaviour depending of the building direction, then orthotropic material cards like ***MAT_157** can be used. The orthotropic stiffness description helps to calculate the deformation behaviour for elastic and low plastic strains. Although the standard material card ***MAT_024** has its limits in describing this special thermoplastics, averaging techniques based on the tension and three point bending test could help to describe at least the behaviour of non-reinforced thermoplastics. On a coupon level, ***MAT_024** showed significant difficulties in describing the anisotropic behaviour of the specimen. Using averaging techniques didn't seem to be effective here. One reason for the averaging difficulties can be the rather homogeneous broad anisotropy of 3D printed materials. When the mounting and loading case act directly parallel to one building direction, as it is the case in coupon tests, averaged material cards can only vaguely depict the behaviour.
Nevertheless, the challenge in prediction the deformation of anisotropic parts did not first arise with 3D printed parts. Compared to the modelling techniques for short-fiber reinforced thermoplastics, the results on a coupon level appear similar. However, component test revealed afterwords, that though the locally predominant anisotropy, averaged isotropic cards like a ***MAT_024**, reached a quite well prediction of the total displacement behaviour [14,15]. With the existing difference between the anisotropies of 3D printed materials and short-fiber reinforced plastics, it has to be evaluated whether calibrated isotropic material cards can also predict the deformation behaviour at component levels.

9 Literature

[1] Stichel, T.; Frick, T.; A Round Robin study for Selective Laser Sintering of polyamide 12: Microstructural origin of the mechanical properties, 2016
[2] Technical data sheet thermoplastics, https://www.kern.de/de/technische-datenblaetter-kunststoffe, date 2019/03/10
[3] Schmid, M.: " Selektives Lasersintern (SLS) mit Kunststoffen", 2015
[4] Technical data sheet, ABS: https://www.stratasys.com/de/materials/search/abs-m30, date 2019/03/10
[5] Technical data sheet, PA2200, EOS: https://eos.materialdatacenter.com/eo/en
[6] Reithofer,P.: "Material Models for Thermoplastics in LS-DYNA from Deformation to Failure", 15th International LS-DYNA Users Conference, 2018, pages 19
[7] Hartmann,S.;Erhart,T.;Haufe,A.: "Short and long fiber reinforced thermoplastics material models in LS-DYNA", DYNAFORUM 2014, Bamberg,pages 23
[8] Jennrich, R.; Roth, M., Kolling, S.: "Experimental and Numerical Analysis of a Glass Fiber Reinforced Plastic", DYNAFORUM 2014, Bamberg, pages 23
[9] LS-DYNA KEYWORD USER'S MANUAL,VOLUME II Material Models,LS-DYNA R10.0,10/16/17 (r:9024)
[10] Haufe,A.;DuBois, P.; Neukamm, F.; Feucht, M.: "GISSMO – Material Modeling with a sophisticated Failure Criteria", LS-DYNA Developer Forum 2011, pages 48
[11] DIN ESN ISO 178: Plastics – Determination of flexural properties (ISO 178:2010 + Amd.1:2013); pages 29
[12] Banabic, D.:"Sheet Metal Forming Processes – Constitutive Modelling and Numerical Simulation", 2009
[13] Korte,W.;Pazour,S.;Stojek,M.: "Potential of MAT157 for Short-Fiber-Reinforced Injection Molded Plastic Components", LS-DYNA FORUM 2016, pages 20
[14] Schöpfer, J.; "Spritzgussbauteile aus kurzfaserverstärkten Kunststoffen: Methoden der Charakteri-ierung und Modellierung zur nichtlinearen Simulation von statischen und crashrelevanten Lastfällen", PhD thesis, 2012
[15] Haufe, A.; Liebold, Ch.: " Zum aktuellen Stand der Simulation von Kunststoffen mit LS-DYNA",4a TT, 2014